Article

J. Biol. Regul. Homeost. Agents. 2024; 38(5): 4239–4251
https://doi.org/10.23812/j.biol.regul.homeost.agents.20243805.336

The PLGA/TCP Scaffold Loaded with Tendon Stem Cells Contributes to the Tendon-Bone Healing of Rotator Cuff Tear in Rabbits

Wei Ding[1,*], Liyong Wei[2], Mingguang Bi[1], Shaohua Ding[1], Jin Li[1]

[1]Orthopedics Department, Ningbo Medical Center Lihuili Hospital, 315041 Ningbo, Zhejiang, China
[2]Medical College, Ningbo University, 315021 Ningbo, Zhejiang, China
*Correspondence: lhldingwei@nbu.edu.cn (Wei Ding)
Published: 1 May 2024

Background: The postoperative healing of rotator cuff tear (RCT) often presents challenges. Poly (lactic-co-glycolic acid)/tricalcium phosphate (PLGA/TCP) scaffold is a composite biomaterial for repairing bone defect. This study aimed to investigate the impact of tendon stem cells (TDSCs)/PLGA/TCP composite scaffold on a rabbit model of RCT.

Methods: After induction using osteogenic, adipogenic and chondrogenic medium, TDSCs differentiation was achieved. The multi-directional differentiation of TDSCs was confirmed through colony formation and staining with alizarin red, oil red, and toluidine blue. Quantitative real-time polymerase chain reaction was utilized to assess the expressions of stemness, osteogenesis, and tendon-related genes. TDSCs were cultured in PLGA/TCP scaffold, and their attachment, markers, and viability were evaluated using immunofluorescence and cell counting kit-8 assay. The rabbit RCT model was made. The morphology and tensile strength of tendon-bone healing were assessed by hematoxylin-eosin, masson, dil staining and tendon stretch assay. Quantification of β-catenin protein was realized by western blot.

Results: The obtained TDSCs were identified as having the ability of multi-directional differentiation and stemness. CD73, CD90, and CD105 were positive and CD45 was negative in TDSCs. The multi-directional differentiation ability of TDSCs was improved on PLGA/TCP scaffold. The TDSC/PLGA/TCP composite scaffold promoted tendon-bone healing, fibrocartilage mineralization and formation, the expressions of osteogenic and tendon-related genes. Furthermore, it significantly promoted β-catenin expression, the invasive number of TDSCs, the ultimate load and stiffness of healing tendon.

Conclusions: The loading of TDSCs further optimized the role of PLGA/TCP scaffold in promoting rotator cuff tendon-bone surface healing, which was closely related to the expression of β-catenin protein.

Keywords: New Zealand white rabbits; PLGA/TCP; tendon stem cells; rotator cuff tear; tendon-bone healing

Introduction

Rotator cuff tear (RCT) is a prevalent shoulder ailment in clinical practice, predominantly occurring in middle-aged and elderly individuals [1–3]. With the progressive aging trend in China, the incidence of RCT has surged [4]. The etiology of RCT primarily encompasses impingement syndrome [5], overuse [6], contractile overload [7], age-related tendon degeneration [8], and aberrant vascular factors [9]. RCT usually can't heal itself. Surgery is often used when conservative treatment is failed or RCT is greater than 50% of normal tendon thickness [10]. However, postoperative healing following repair is accompanied by a high failure rate [11,12]. Furthermore, RCT frequently manifests at the tendon-bone junction, the critical interface between musculature and bone tissues [13]. Presently, the challenges of rotator cuff re-tearing and inadequate healing at the tendon-bone interface persist unsolved. Consequently, enhancing the healing of the rotator cuff tendon-bone surface necessitates the reconstruction of a multilayer fibrocartilaginous structure, representing a pivotal step in RCT repair.

Recently, numerous professional scholars have embarked on novel endeavors to address RCT repair. Mesenchymal stem cells (MSCs) have emerged as potential agents for treating rotator cuff injuries [14]. However, the use of MSCs alone may prove insufficient for bone defect repair [15]. Notably, the combination of poly (lactic-co-glycolic acid) (PLGA) scaffold and bone marrow-derived mesenchymal stem cells has shown promise in promoting tendon-bone healing in the rabbit model of RCT [16]. PLGA is a biological medicine material, which is biodegradable and no side effects [17]. Specifically, the PLGA/tricalcium phosphate (TCP) scaffold is a promising composite biomaterial for bone defect repair, addressing the limitations of sole stem cell therapy for treating rotator cuff injuries [18]. The primary advantages of PLGA/TCP scaffold include degradability, cost-effectiveness, and accessi-

Journal of
BIOLOGICAL REGULATORS
and Homeostatic Agents

bility. TCP induces osteogenic differentiation of stem cells and enhances heterotopic ossification [19]. Previous research reveals that wollastonite/TCP scaffold repairs bone defect in rat calvaria [20]. Currently, optimized methods for RCT treatment primarily involve the implantation of osteogenic induction materials (such as TCP or degradable scaffolds) and the administration of related growth factors (such as bone morphogenetic protein 2 and platelet-rich plasma) at the injury site [21]. Therefore, PLGA/TCP scaffold has a potential application to repair RCT.

Moreover, the integration of stem cells has novel avenues for treating RCT. Stem cells exist in various adult tissues, including tendon stem cells (TDSCs) [22]. TDSCs exhibit robust directional differentiation capabilities [23]. Research indicates that adipose-derived stem cells promote RCT repair by facilitating the osteogenic differentiation of TDSCs [24]. The activation of the β-catenin signaling pathway induces osteogenic differentiation of bone marrow mesenchymal stem cells, which is beneficial for RCT repair [25]. Theoretically, TDSCs may enhance tendon-bone healing and improve tendon function. However, the clinical applicability of this approach remains unknown [26]. Currently, research on biomaterials primarily focuses on promoting bone regeneration to enhance the connection strength between tendon and bone. We aimed to explore the potential of TDSCs and tissue engineering for clinical RCT treatment.

In general, our study aimed to evaluate the impact of TDSC/PLGA/TCP composite scaffold on the rabbit RCT model. Additionally, we aimed to investigate whether PLGA/TCP scaffold loaded with TDSCs could influence the multi-directional differentiation of TDSCs and elucidate the relevant molecular mechanisms.

Materials and Methods

Animals

Forty male New Zealand white rabbits, aged 10 weeks and weighing 1.6–1.8 kg, were obtained from Shanghai Jiagan Biotechnology (Shanghai, China). The rabbits were housed at room temperature (RT) with 45% humidity and a 12-hour light-dark cycle. They were provided ad libitum access to food and water throughout the experimental period. All experimental procedures involving New Zealand white rabbits were conducted following the China Council on Animal Care and Use guidelines and were approved by the Ethics Committee of Ningbo University for Experimental Animals Welfare (Approval No. 2019-151).

Isolation and Culture of Rabbit Supraspinatus TDSCs

Eight New Zealand white rabbits were anesthetized using urethane (A600448; Sangon Biotech, Shanghai, China) at a dosage of 1.2 g/kg [27]. Following anesthesia, the hair covering the rotator cuff was shaved, and the skin was disinfected. Under aseptic conditions, the supraspinatus tendon was carefully isolated and then immersed in 1× PBS (P1020; Solarbio, Beijing, China) supplemented with 1% streptomycin/penicillin (15140122; Thermo Fisher Scientific, Waltham, MA, USA). The tendon tissue was diced into 1 mm^3 fragments. Subsequently, 0.2% collagenase type I (A004194; Sangon Biotech, Shanghai, China) was used to isolate tendon cells in α-minimal essential medium (α-MEM; SH30265.01; HyClone, Logan, UT, USA) at 37.5 °C for 4 hours. The resulting cells were characterized as supraspinatus tendon stem cells (TDSCs).

A total of 5000 TDSCs were seeded into a 10 cm culture dish. The cells were cultured in α-MEM supplemented with 10% fetal bovine serum (FBS; 10100147; Thermo Fisher Scientific, Waltham, MA, USA) and 0.1% penicillin/streptomycin at 37 °C in a 5% CO_2 atmosphere for 10 days. The culture medium was refreshed every 3 days. The morphology of TDSCs was observed and photographed using a light microscope (magnification, ×200; LV150; Nikon Inc., Tokyo, Japan).

Multi-Directional Differentiation of TDSCs

The second generation of TDSCs (2×10^4 cells) was seeded into 6-well plates. Upon reaching 80% confluence, the cells were subjected to differentiation induction using osteogenic induction medium (CTCC-Y001, Wuxi Puhe Biomedical Technology Inc., Wuxi, China), adipogenic induction medium (CTCC-Y003, Wuxi Puhe Biomedical Technology Inc., Wuxi, China), or chondrogenic induction medium (CTCC-Y002, Wuxi Puhe Biomedical Technology Inc., Wuxi, China) at 37 °C in a 5% CO_2 atmosphere for 7 days [23].

Cell Grouping

Following culturing in standard, osteogenic, adipogenic, or chondrogenic induction media, TDSC cells were divided into four groups: Uninduced, Osteogenesis, Adipogenic, and Chondrogenic groups [23].

Subsequently, based on whether TDSCs or multi-directional differentiation TDSCs were treated with the PLGA/TCP scaffold, six groups were established: Without scaffold, Scaffold Only, without scaffold and Induced, Scaffold and Osteogenesis, Scaffold and Adipogenic, and Scaffold and Chondrogenic groups, respectively.

RCT Model in Rabbits

Thirty-two New Zealand white rabbits (eight rabbits in each group) were anesthetized using urethane at a dosage of 1.2 g/kg [27]. Under aseptic conditions, the skin overlying the rabbit rotator cuff was incised, and the deltoid was dissected. A bone tunnel (0.5 mm) was drilled from the front to the back through the greater tuberosity to create the RCT model [16]. Subsequently, all RCT rabbits were allocated to different treated groups. Control group: After establishing the RCT model, no further treat-

ment was administered. TDSC group: Following establishing the RCT model, a suspension of TDSCs (1×10^7 cells/mL, 20 µL) was injected into the anastomotic site [28]. PLGA/TCP group: After establishing the RCT model, a PLGA/TCP scaffold was implanted at the anastomotic site. TDSC/PLGA/TCP group: Following establishing the RCT model, a TDSC/PLGA/TCP composite scaffold was implanted at the anastomotic site. The number of TDSCs was 1×10^7 cells/mL (20 µL) per scaffold layer (total of two layers). Subsequently, the supraspinatus tendon-bone junction was sutured.

At 4th and 12th weeks post-surgery, the anastomosed supraspinatus tendon tissues were excised and fixed with 4% paraformaldehyde for 12 hours. The tendon tissues were placed in a 50 mL centrifuge tube filled with 10% ethylene diamine tetraacetic acid (EDTA) decalcification solution (DD002; Solarbio, Beijing, China) for 4 weeks. When there was no obvious resistance to penetrate the tissue with the syringe needle, the decalcification was complete. Finally, the tendon tissues were embedded with paraffin (A601888; Sangon Biotech, Shanghai, China) and sectioned for further analysis.

Alizarin Red Staining Assay

The Alizarin Red staining kit (CTCC-JD001; Wuxi Puhe Biomedical Technology Inc., Wuxi, China) was utilized to assess osteogenic differentiation. Induced TDSCs were fixed with stationary solution (500 µL) at 37 °C for 30 minutes. After two washes with PBS, Alizarin Red staining solution (500 µL) was added to the cells for 20 minutes at 37 °C. Following three additional washes with PBS, osteoblast differentiation of TDSCs was visualized using a light microscope (magnification, ×200; LV150; Nikon Inc., Tokyo, Japan).

Oil Red Staining Assay

The oil red staining kit (CTCC-JD003; Wuxi Puhe Biomedical Technology Inc., Wuxi, China) was employed to assess adipogenic differentiation. The oil red staining solution was prepared as follows: The oil red staining solution and staining diluent were mixed in a ratio of 3:2 and allowed to stain at room temperature for 10 minutes. Induced TDSCs were fixed with stationary solution (500 µL) at 37 °C for 30 minutes. After two washes with washing solution I (500 µL), the cells were incubated with the oil red working solution (500 µL) at 37 °C for 20 minutes. Following two washes with washing solution III (500 µL), and solution II (500 µL), the adipogenic differentiation of TDSCs was visualized using a light microscope (magnification, ×200; LV150; Nikon Inc., Tokyo, Japan).

Toluidine Blue Staining Assay

The toluidine blue staining kit (E670105; Sangon Biotech, Shanghai, China) was employed to detect chondrogenic differentiation. The preparation of the 0.1% toluidine blue staining working solution was as follows: the toluidine blue staining solution (1%) was mixed with diluent in a ratio of 1:9. TDSCs were collected and smeared onto glass slides. Subsequently, the cells were fixed with 4% paraformaldehyde (P0099; Beyotime, Shanghai, China) for 20 minutes at 25 °C. Finally, the 0.1% toluidine blue staining working solution was applied to dye cells for 2 minutes. After drying, the chondrogenic differentiation of TDSCs was visualized using a light microscope (magnification, ×200; LV150; Nikon Inc., Tokyo, Japan).

Immunofluorescence Assay

The TDSCs were seeded onto cover glass and fixed with 4% paraformaldehyde for 30 minutes. Subsequently, the cells were washed three times with 1× PBS for 10 minutes each. TDSCs were transparentized by Triton X-100 (P0096; Beyotime, Shanghai, China) for 10 minutes. Immunostaining blocking buffer (P0102; Beyotime, Shanghai, China) was added to the samples and incubated for 1 hour. Primary antibodies against octamer binding transcription factor 4 (OCT-4; ab137427; 1:100; Abcam, Cambridge, UK), nucleostemin (#GT15050; 1:400; Neuromics, Edina, MN, USA), CD45 (ab303670, 1:500; Abcam, Cambridge, UK), CD73 (ab288154, 1:500; Abcam, Cambridge, UK), CD90 (ab133350, 1:50; Abcam, Cambridge, UK), and CD105 (ab221675, 1:1000; Abcam, Cambridge, UK) were then added to the sample and incubated at 4 °C overnight. Following primary antibody incubation, the samples were incubated with secondary antibodies (ab150077, Alexa Fluor® 488; ab150115, Alexa Fluor® 647; 1:1000; Abcam, Cambridge, UK) at 25 °C for 2 hours in the dark. Additionally, the stage-specific embryonic antigen 4 (SSEA-4; ab16287; Alexa Fluor 647; 1:100; Biovision, Milpitas, CA, USA) antibody was applied to the samples and incubated overnight at 4 °C in the dark. Antifade mounting medium with 4,6-diamino-2-phenyl indole (DAPI; P0131; Beyotime, Shanghai, China) was used to prevent fluorescence quenching. Finally, images were captured using a confocal fluorescent microscope (magnification, ×200; TCS SP8; Leica Camera AG Inc., Solms, Germany).

Quantitative Real-Time Polymerase Chain Reaction (qRT-PCR)

Total RNA from TDSCs or multi-directional differentiation TDSCs, treated with or without the PLGA/TCP scaffold, or tendon tissue was extracted using the Trizol kit (B511311; Sangon Biotech, Shanghai, China). The RNA concentration was determined using the Evolution 260 Bio Spectrophotometer (840-211000; Thermo Fisher Scientific, Waltham, MA, USA). The FastQuant RT kit (KR106-03; Tiangen Biotech, Beijing, China) was employed to synthesize cDNA. Amplified cDNA was quantified using the Dynamo ColorFlash SYBR Green kit (F-416L; Thermo Fisher Scientific, Waltham, MA, USA). Prepared samples were

Journal of
BIOLOGICAL REGULATORS
and Homeostatic Agents

Table 1. The primer sequences of related genes.

Genes	Forward primer	Reverse primer
RUNX-2	GGCGCATTTCAGGTGCTTC	ATACCGCTGGACCACTGTTG
PPARγ	GGGTTGACCCTGAGAACCTC	TAATCCGCAACCATGGGGTC
COL-2a1	TTCCTCCTCCTGCTCCCAG	GAGCCACTCTCACCCTTCAC
ALPL	TTTGTCTGGAACCGCACTGA	TCCTGTTCAGCTCGTACTGC
COL-1a1	CGATGGCTTCCAGTTCGAGT	TCGTGGAGGACAGTGTAGGT
Scx	CAGACGGACGTACAGACAGG	GAAAAGCCAGCGCAGAAAGT
TNC	GGGATTAATGTCGGAAATGGT	CCGGACCAAAACCATCAGT
GAPDH	GGCAAAGTGGATGTTGTCGC	GCCGTGGGTGGAATCATACT

RUNX-2, runt-related transcription factor 2; *PPARγ*, peroxisome proliferator-activated receptor γ; *COL-2a1*, collagen-type II alpha 1; *ALPL*, alkaline phosphatase; *COL-1a1*, collagen-type I alpha 1; *TNC*, Tenascin C; *GAPDH*, glyceraldehyde-3-phosphate dehydrogenase.

analyzed using a qRT-PCR instrument (MJOpticon2, Bio-Rad Inc., Hercules, CA, USA). The data were analyzed using the $2^{-\Delta\Delta Ct}$ [29], with glyceraldehyde-3-phosphate dehydrogenase (*GAPDH*) as the internal reference. The primers used are listed in Table 1 and were synthesized by Sangon Biotech (Shanghai, China).

Preparation of PLGA/TCP Scaffold

The PLGA/TCP scaffold was prepared following a previously established protocol with minor modifications [30]. First, 1,4-Dioxane (A604300; Sangon Biotech, Shanghai, China) was used to prepare solutions of 8% PLGA and 2% TCP. Subsequently, the 8% PLGA and 2% TCP solutions were mixed in a 1:1 volume ratio and stirred at 4 °C overnight. The resulting mixture of PLGA and TCP (3 mL) was dispensed into 24-well plates and subjected to freeze-drying at –60 °C for 6 hours. The diameter of the resulting PLGA/TCP scaffold was approximately 15.6 mm. The morphological structure and characteristics of the PLGA/TCP scaffold were examined using a scanning electron microscope (magnification, ×100, ×1000, and ×10,000; Quanta250; FEI Inc., Hillsboro, OR, USA).

Seeding of TDSCs onto PLGA/TCP Scaffold

The PLGA/TCP scaffold was first incubated in 70% ethanol for 12 hours. 70% ethanol was obtained from diluent anhydrous ethanol (A500737; Sangon Biotech, Shanghai, China). After drying, the PLGA/TCP scaffold was immersed in α-MEM for 1 week. Subsequently, TDSCs (1×10^5 cells) were seeded onto the PLGA/TCP scaffold for 4 hours at 37 °C with 5% CO_2 for further experiments.

Cell Counting Kit-8 (CCK-8) Assay

TDSCs (1×10^4 cells) were seeded onto 96-well plates or the PLGA/TCP scaffold. Cell viability was evaluated using the CCK-8 kit (C0039; Beyotime, Shanghai, China). At days 1, 3, and 5, TDSCs were harvested and incubated with CCK-8 reagent (10 μL) at 37 °C for 2 hours. Subsequently, the absorbance at 450 nm was measured using a microplate reader (VLBL0TD2; Thermo Fisher Scientific, Waltham, MA, USA).

Cell Nucleus Blue Fluorescence Staining Assay

The cell nuclei of TDSCs were labeled using DAPI staining solution (C1006; Beyotime, Shanghai, China). TDSCs were cultured on the PLGA/TCP scaffold for 15 days. Subsequently, the TDSCs were fixed with 4% paraformaldehyde for 20 minutes at 25 °C. Following the manufacturer's instructions, the cells were washed twice with 1× PBS, and then the cell nucleus staining solution (500 μL) was added to the cells in darkness and incubated at 25 °C for 5 minutes. Finally, the blue fluorescent-labeled TDSCs were imaged using a confocal fluorescent microscope (magnification, ×200; TCS SP8; Leica Camera AG Inc., Solms, Germany).

Hematoxylin-Eosin (HE) Staining Assay

The morphological structure of tendon healing at the anastomotic site was examined using the HE staining kit (C0105M; Beyotime, Shanghai, China). Following embedding in paraffin and sectioning, the tendon tissue was dewaxed twice with xylene (A530011; Sangon Biotech, Shanghai, China) for 10 minutes each. Subsequently, the tissue sections were rehydrated with water and stained with hematoxylin staining solution for 10 minutes, then rinsed with tap water for 10 minutes to remove the excess staining solution. The tendon tissue was then stained with eosin staining solution for 1 minute and dehydrated. After dehydration, the tendon tissue was cleared twice with xylene for 5 minutes each. Neutral gum (E675007; Sangon Biotech, Shanghai, China) was used to seal the tissue. Finally, the tendon tissue was photographed by a light microscope (magnification, ×100; LV150; Nikon Inc., Tokyo, Japan).

Table 2. Antibodies used in this study.

Name	Catalog	Molecular weight	Dilution	Manufacturer
β-catenin	ab227499	85 kDa	1/10,000	Abcam, Cambridge, UK
GAPDH	ab125247	36 kDa	1/5000	Abcam, Cambridge, UK
Goat anti rabbit	ab97051	—	1/10,000	Abcam, Cambridge, UK
Goat anti mouse	ab96879	—	1/10,000	Abcam, Cambridge, UK

Masson Staining Assay

The organization of the tendon-bone interface was assessed using the masson trichrome stain kit (G1340; Solarbio, Beijing, China). Following dewaxing, the tissues were stained with Weigert iron hematoxylin staining solution for 10 minutes. Subsequently, the tissues were differentiated using an acidic ethanol differentiation solution for 15 seconds, then rinsed and stained with masson blue solution for 5 minutes. After rinsing with distilled water for 1 minute, the tissues were stained with ponceau magenta staining solution for 10 minutes. Sequentially, the tissues underwent orderly washing with molybdenum pickling solution and a weak acid working solution for 1 minute. The tissues were then immersed in aniline blue staining solution for 2 minutes and subsequently washed with a weak acid working solution for 1 minute. Following the washing, the tissues were rapidly dehydrated with 95% ethanol (A507050; Sangon Biotech, Shanghai, China) for 3 seconds and with anhydrous ethanol (A500737; Sangon Biotech, Shanghai, China) for 5 seconds (repeated three times). Subsequently, the tissues were cleared with xylene for 2 minutes (repeated three times). Finally, neutral gum was used to seal the tissues. The stained tissues were observed under a light microscope (magnification, $\times$100; LV150; Nikon Inc., Tokyo, Japan).

Western Blot Analysis

Tendon tissue from all groups was collected and ground to extract total protein. Total protein extraction was performed using an extraction kit (C006225; Sangon Biotech, Shanghai, China), and its concentration was determined using a concentration assay kit (P0010; Beyotime, Shanghai, China). Gel reagents (P0012A; P0690; Beyotime, Shanghai, China) were used to separate proteins, which were then transferred onto 0.45 mm membranes (FFP32; Beyotime, Shanghai, China). After blocking with 5% fat-free milk for 1 hour at 25 °C, the membranes were incubated with primary antibodies overnight at 4 °C, followed by incubation with secondary antibodies for 1 hour at 25 °C. Glyceraldehyde-3-phosphate dehydrogenase (GAPDH) was used as the internal reference. Protein blots were detected using electro-chemi-luminescence (ECL) reagent (32209; Thermo Fisher Scientific, Waltham, MA, USA) and captured using a gel imaging analysis system (GeneGenius; Baijing Biotechnology Inc., Beijing, China). The antibodies used are listed in Table 2.

Dil Staining Assay

TDSCs were labeled with a cell membrane red fluorescent staining reagent (C1991S; Beyotime, Shanghai, China). Briefly, cell membrane staining solution (500 µL) was added to the cells, and they were incubated at 37 °C for 20 minutes in the dark. After washing the cells twice with 1$\times$ PBS, preheated medium at 37 °C was added to the cells. Finally, the red fluorescent-labeled TDSCs were visualized and imaged using a confocal fluorescent microscope (magnification, $\times$200; TCS SP8; Leica Camera AG Inc., Solms, Germany).

Tendon Stretch Assay

The tensile strength was measured using an Instron testing system (5980; Instron Inc., Norwood, MA, USA). After anesthetized (100 mg/kg pentobarbital, P3761, Sigma-Aldrich, Darmstadt, Germany), rabbits were euthanized by cervical dislocation, regenerated tendon tissues were collected from rabbits treated with or without TDSCs, PLGA/TCP scaffold, or TDSC/PLGA/TCP compound scaffold. According to early study, the regenerated tendon tissue was preloaded to 0.1 N. Then, every tendon tissue was loaded to maximum at a speed of 50 mm/min [16]. The ultimate load and stiffness were analyzed using the Instron testing systems to assess tensile strength.

Statistical Analysis

All statistical analyses were conducted using GraphPad Prism 8.0 (GraphPad Software Inc., San Diego, CA, USA). The data were presented as mean $\pm$ standard deviation. Categorical variables were compared using the χ^2 test. Data normality was assessed using the Shapiro-Wilk test. Independent one-way ANOVA with Tukey multiple comparisons was performed for normally distributed quantitative parameters. One-way ANOVA was utilized to compare multiple groups. Statistical significance was considered at $p < 0.05$.

Results

Multi-Directional Differentiation Capacity and Stemness of Obtained TDSCs

The obtained TDSCs were cultured, forming clustered cell colonies with irregular morphology and polygonal shape. Nuclei were centralized, with cytoplasmic protrusions extending radially outward (Fig. 1A,a). Staining results confirmed the successful identification of TD-

Journal of
BIOLOGICAL REGULATORS
and Homeostatic Agents

SCs capable of osteogenic, adipogenic, and chondrogenic differentiation (Fig. 1A,b–d). Immunofluorescence assays revealed positive expression of stem cell markers, including OCT-4, SSEA-4, and nucleostemin, in TDSCs (Fig. 1B). Additionally, CD73, CD90, CD105 were positive and CD45 was negative in TDSCs (Fig. 1C). Furthermore, combined with qRT-PCR results, the mRNA levels of runt-related transcription factor 2 (*RUNX-2*), peroxisome proliferator-activated receptor γ (*PPAR*γ), and collagen-type II alpha 1 (*COL-2a1*) were signally increased in multi-directional differentiation TDSCs (Fig. 2A, $p < 0.001$). These findings indicate the successful induction of TDSCs into osteogenic, adipogenic, and chondrogenic cells.

Enhanced Multi-Directional Differentiation Ability of TDSCs on PLGA/TCP Scaffold

Scanning electron microscopy revealed the porous nature of the original PLGA/TCP surface, with clearly visible trabecular and macropores, confirming successful scaffold fabrication (Fig. 2B,B1,B2). Upon magnification, a significant number of micropores were observed on the trabecular surface (Fig. 2B,B3,B4). TDSCs were attached to the PLGA/TCP scaffolds 4 hours after seeding. Fig. 3A depicts numerous blue fluorescent-labeled TDSCs adhering to the surface of the PLGA/TCP scaffold pores. Subsequently, the viability of TDSCs on the scaffolds at days 1, 3, and 5 post-seeding is shown in Fig. 3B. The results indicated no significant difference between the Without scaffold and Scaffold groups (Fig. 3B). Furthermore, compared to the scaffold-free group, qRT-PCR analysis revealed upregulation of *RUNX-2* and *COL-2a1* in the PLGA/TCP scaffold-exposed group (Fig. 3C, $p < 0.001$), while *PPAR*γ level remained unchanged (Fig. 3C). These findings suggest that the PLGA/TCP scaffold provides a favorable environment to promote osteogenic and chondrogenic differentiation of TDSCs.

TDSC/PLGA/TCP Composite Scaffold Promotes Tendon-Bone Healing, Fibrocartilage Mineralization, and Levels of Osteogenesis and Tendon-Related Genes

Combined with above results, the role of TDSC *in vivo* was assessed. The RCT model was made in rabbits, and prepared scaffolds were implanted into the anastomotic site (Fig. 4A). Hematoxylin-eosin (HE) staining results at 4 weeks showed that compared to the Control group, TDSC or PLGA/TCP groups, TDSC/PLGA/TCP composite scaffold promoted fibrocartilage, scar hyperplasia, and decreased granulation space (Fig. 4B). By the 12th week, compared to the Control, TDSC, or PLGA/TCP groups, it can be seen that fibrocartilage was increased, fibrous layers were tight, and healing was better in the TDSC/PLGA/TCP composite scaffold group (Fig. 4B), indicating that TDSC/PLGA/TCP composite scaffold promoted tendon healing in anastomotic site

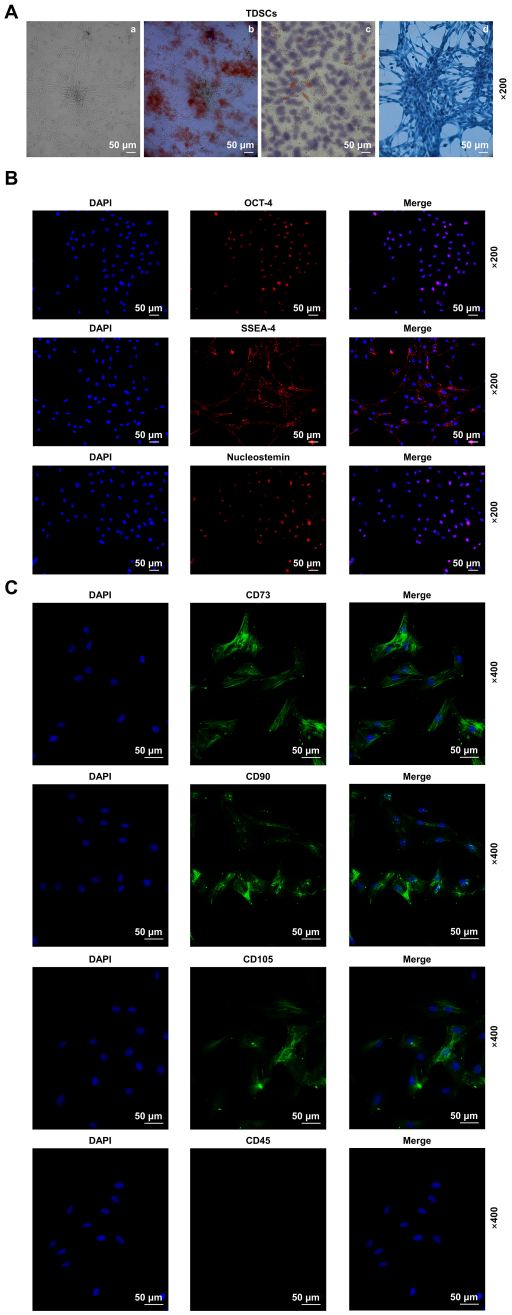

Fig. 1. Verification of multi-directional differentiation and stemness in TDSCs. (A) Morphology and multi-directional differentiation of TDSCs were assessed by light microscope (a), alizarin red staining (b), oil red staining (c), and toluidine blue staining (d). Magnification: ×200, scale bar: 50 μm. (B) Immunofluorescence assay was used to evaluate the stemness of TDSCs. Magnification: ×200, scale bar: 50 μm. (C) Immunofluorescence assay was used to assess the expression of TDSC markers. Magnification: ×400, scale bar: 50 μm. Each experiment was performed three times (n = 3). Abbreviations: TDSCs, tendon stem cells; DAPI, 4,6-diamino-2-phenyl indole; OCT-4, octamer binding transcription factor 4; SSEA-4, stage-specific embryonic antigen 4.

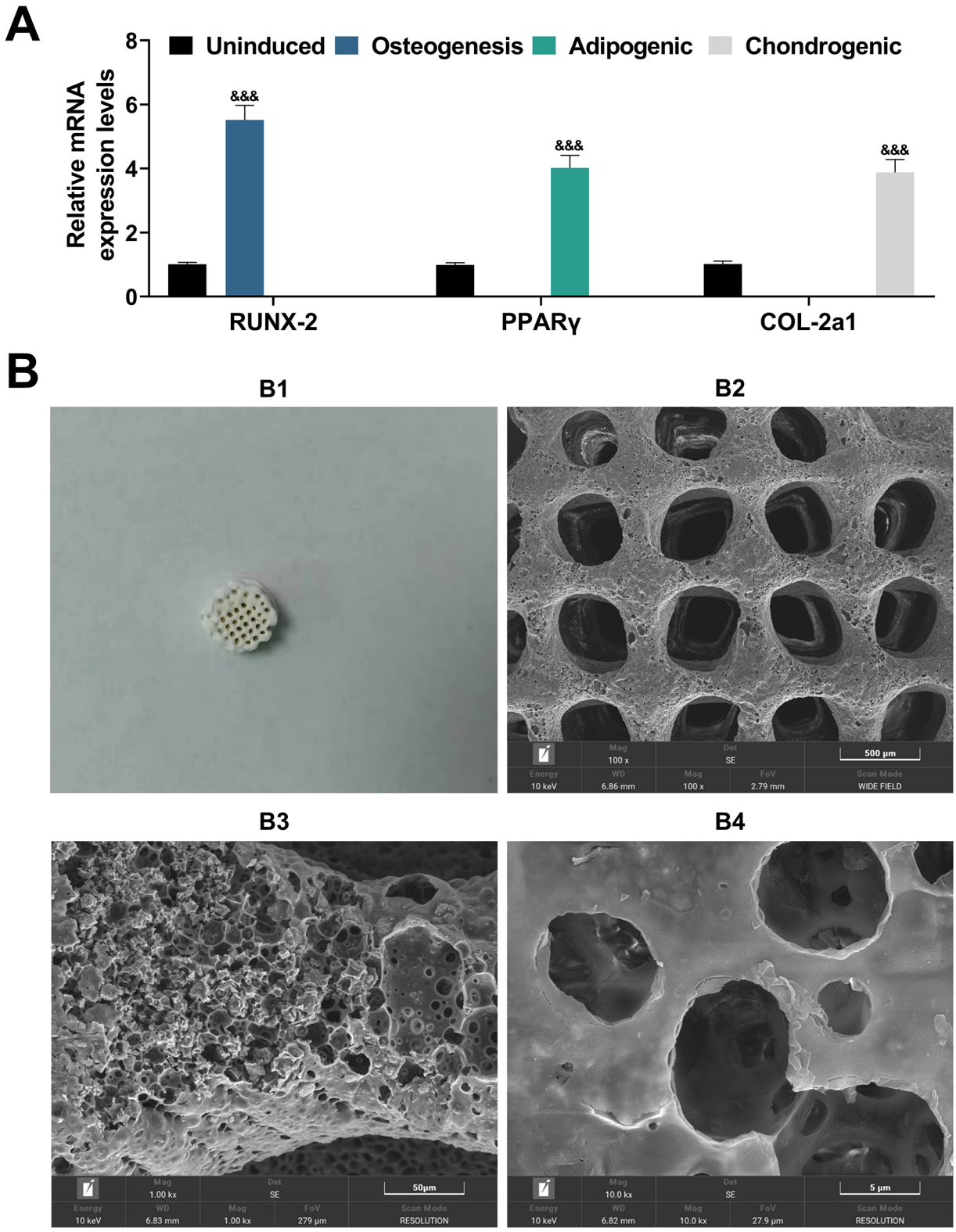

Fig. 2. Expression levels of *RUNX-2*, *PPARγ*, and *COL-2a1* in multi-directional differentiation TDSCs. (A) The mRNA expression levels of *RUNX-2*, *PPARγ*, and *COL-2a1* after multi-directional differentiation of TDSCs were assessed by qRT-PCR, with *GAPDH* as the internal reference. (B) Image of PLGA/TCP scaffold (B1) (scanning electron microscope). (B2) Scale bar: 500 µm, magnification ×100. (B3) Scale bar: 50 µm, magnification: ×1000. (B4) Scale bar: 5 µm, magnification: ×10,000. $^{\&\&\&}p < 0.001$ vs. Uninduced group. Each experiment was conducted three times (n = 3). Abbreviations: *PPARγ*, peroxisome proliferator-activated receptor ϒ; qRT-PCR, quantitative real-time polymerase chain reaction; PLGA/TCP, poly (lactic-co-glycolic acid)/tricalcium phosphate.

Journal of
BIOLOGICAL REGULATORS
and Homeostatic Agents

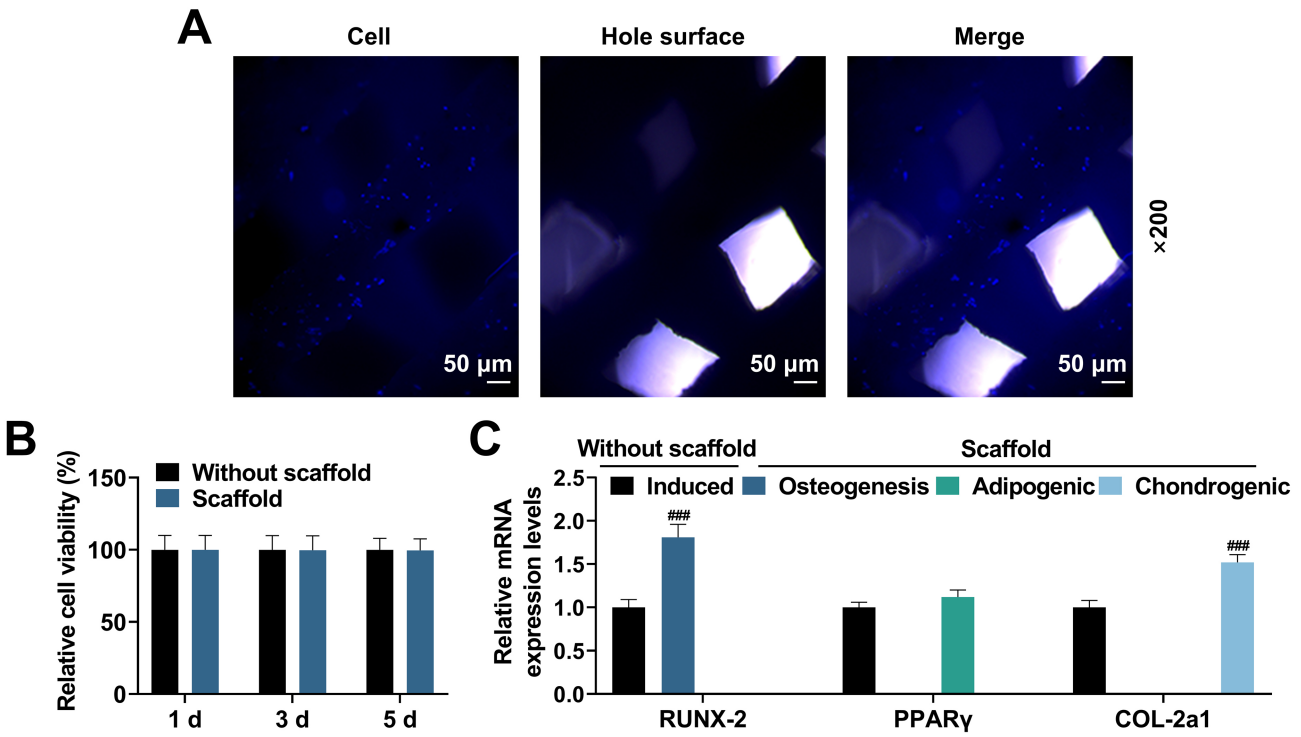

Fig. 3. Enhancement of multi-directional differentiation ability of TDSCs on PLGA/TCP scaffold. (A) Image of blue fluorescent labeled TDSCs after attaching the TDSCs to PLGA/TCP scaffolds (a confocal fluorescent microscope). Scale bar: 50 μm, magnification: ×200. (B) TDSCs viability on PLGA/TCP scaffold (Cell Counting Kit-8 (CCK-8) assay). (C) mRNA expression levels of *RUNX-2, PPARγ,* and *COL-2a1* after attachment of TDSCs to PLGA/TCP scaffold and induction of differentiation with osteogenic, adipogenic, and chondrogenic induction medium, respectively, were analyzed by qRT-PCR, with *GAPDH* as the internal reference. $^{###}p < 0.001$ vs. Without scaffold-induced group. Each experiment was conducted three times (n = 3). Abbreviations: d, day.

(Fig. 4B). Moreover, compared to the Control, TDSC or PLGA/TCP groups, masson staining results indicated that the TDSC/PLGA/TCP composite scaffold enhanced fibrocartilage proliferation, mineralization, and collagen content and also increased the number and density of fibrocytes (Fig. 4C).

Furthermore, compared to the Control group, qRT-PCR results revealed significantly increased expressions of osteogenesis-related genes (*RUNX-2*, alkaline phosphatase (*ALPL*), and collagen-type I alpha 1 (*COL-1a1*)) and tendon-related genes (*Scx* and Tenascin C (*TNC*)) in the TDSC, PLGA/TCP group (Fig. 5A–E, $p < 0.01$). Notably, compared to the TDSC or PLGA/TCP group, the TDSC/PLGA/TCP composite scaffold significantly upregulated the expressions of *RUNX-2*, *ALPL*, *COL-1a1*, *Scx,* and *TNC* (Fig. 5A–E, $p < 0.001$). These findings suggest that the TDSC/PLGA/TCP composite scaffold exhibits superior efficacy in tendon-bone healing.

TDSC/PLGA/TCP Composite Scaffold Promotes β-Catenin Expression, the Invasive Number of TDSC, and the Ultimate Load and Stiffness of the Healing Tendon

Compared to the TDSC or PLGA/TCP group, the western blot results revealed a significant upregulation of β-catenin protein by the TDSC/PLGA/TCP composite scaffold (Fig. 6A,B, $p < 0.001$). Relative to the Control group, the expression of β-catenin protein was also significantly increased by TDSC (Fig. 6A,B, $p < 0.001$), but no significant difference was observed with PLGA/TCP. Moreover, compared to the PLGA/TCP group, the results of dil staining revealed an increased infiltration of TDSCs in the tendon in the TDSC/PLGA/TCP composite scaffold group (Fig. 6C). The TDSC group had certain TDSC display (Fig. 6C). Furthermore, compared to the TDSC or PLGA/TCP group, the results of the tendon stretch assay demonstrated a significant increase in the ultimate load and stiffness of the healing tendon by the TDSC/PLGA/TCP composite scaffold (Fig. 6D,E, $p < 0.01$). Compared to the Control group, the ultimate load and stiffness of the healing tendon were increased by TDSCs (Fig. 6D,E, $p < 0.05$). Additionally, compared to the Control group, the stiffness of the healing tendon was increased by PLGA/TCP (Fig. 6E, $p < 0.05$), although the ultimate load was minimally affected (Fig. 6D).

Discussion

RCT is a kind of frequent disease in clinic, mainly depending on the treatment of surgery [31]. However, with

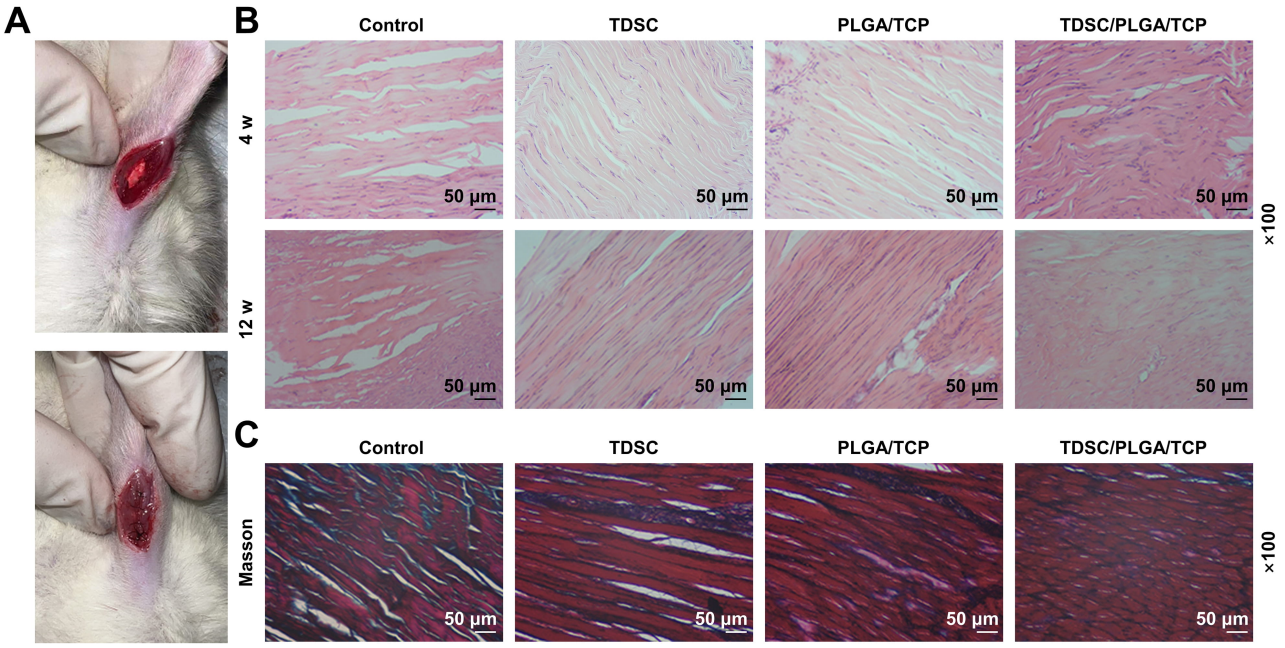

Fig. 4. TDSC/PLGA/TCP composite scaffold promotes tendon-bone healing, fibrocartilage mineralization and formation. (A) Implantation of composite scaffold materials in the tendon (above) and suture (below). (B) Morphology of the tendon anastomotic site in the RCT model was revealed by HE staining assay. Scale bar: 50 μm, magnification: ×100. (C) Morphology of the tendon-bone anastomotic site in the RCT model was demonstrated by masson staining assay. Scale bar: 50 μm, magnification: ×100. Abbreviations: w, week; HE, hematoxylin-eosin; RCT, rotator cuff tear. Each experiment was conducted eight times (n = 8).

increasing age, the efficacy of surgy tends to diminish [32]. The tendon, a critical component of the rotator cuff, connects bone and muscle [33]. Due to poor prognosis, it is still a clinical challenge for musculoskeletal regeneration in injured tendon. Recently, the integration of endogenous/progenitor stem cells with tissue engineering has emerged as a promising approach for repairing rotator cuff injuries [34]. Furthermore, biological scaffolds combined with stem cells may be an effective therapy to repair rotator cuff tendon-bone surface healing. The biomechanical properties of biological scaffolds and stem cells are alike to the native tissue [35]. In our study, TDSCs were obtained from tendon tissue. Notably, our outcomes revealed that the loading of TDSCs further optimized the role of PLGA/TCP scaffold in promoting rotator cuff tendon-bone surface healing.

In recent years, extensive studies have investigated the role of stem cells in the repair of rotator cuff injury and tendon-bone healing [36,37]. Combined with our results, the properties of multi-directional differentiation and stemness were identified in TDSCs. Through induction of osteogenic, adipogenic and chondrogenic media, TDSCs were differentiated toward osteogenesis, adipogenesis and chondrogenesis. Furthermore, the expressions of stemness-related genes (*OCT-4*, *SSEA-4*, and nucleostemin) were positive. TDSCs promote tendon growth, maintenance, and repair [38]. At the rotator cuff repair site, the number of TDSCs in tendon is more than that in bone [39]. Additionally, mesenchymal stem cells enhance tendon-bone healing *in vivo* [40]. However, the specific impact of TDSCs on tendon-bone healing remains incompletely understood. Therefore, we posit that TDSCs possess the potential to repair RCT and promote tendon-bone healing.

Additionally, the increasing utilization of biological scaffolds can enhance repair capacity in RCT [41]. In our study, TDSCs were successfully cultured on a PLGA/TCP scaffold, which promoted the expressions of *RUNX-2* (representing osteogenesis) and *COL-2a1* (representing chondrogenesis) in TDSCs. PLGA scaffold, known for its favorable biocompatibility and biodegradability, is widely applied in bone tissue engineering [42]. Particularly, PLGA/TCP scaffold has demonstrated efficacy in repairing various bone defects [43]. Furthermore, composite scaffolds such as PLGA/TCP/phytomolecule icaritin have been shown to promote bone regeneration in rat models [44]. However, the specific impact of PLGA/TCP scaffold on RCT remains unclear. Our findings suggest that the PLGA/TCP scaffold could promote the multi-directional differentiation of TDSCs, potentially enhancing rotator cuff repair and tendon-bone healing.

Recent research has revealed that a combination of biological scaffolds and stem cells may be an effective therapeutic approach for repairing RCT [45]. Our outstanding contribution in this research was that TDSC/PLGA/TCP composite scaffold promoted RCT repair and tendon-done healing in rabbit model by activating β-catenin signaling

Journal of
BIOLOGICAL REGULATORS
and Homeostatic Agents

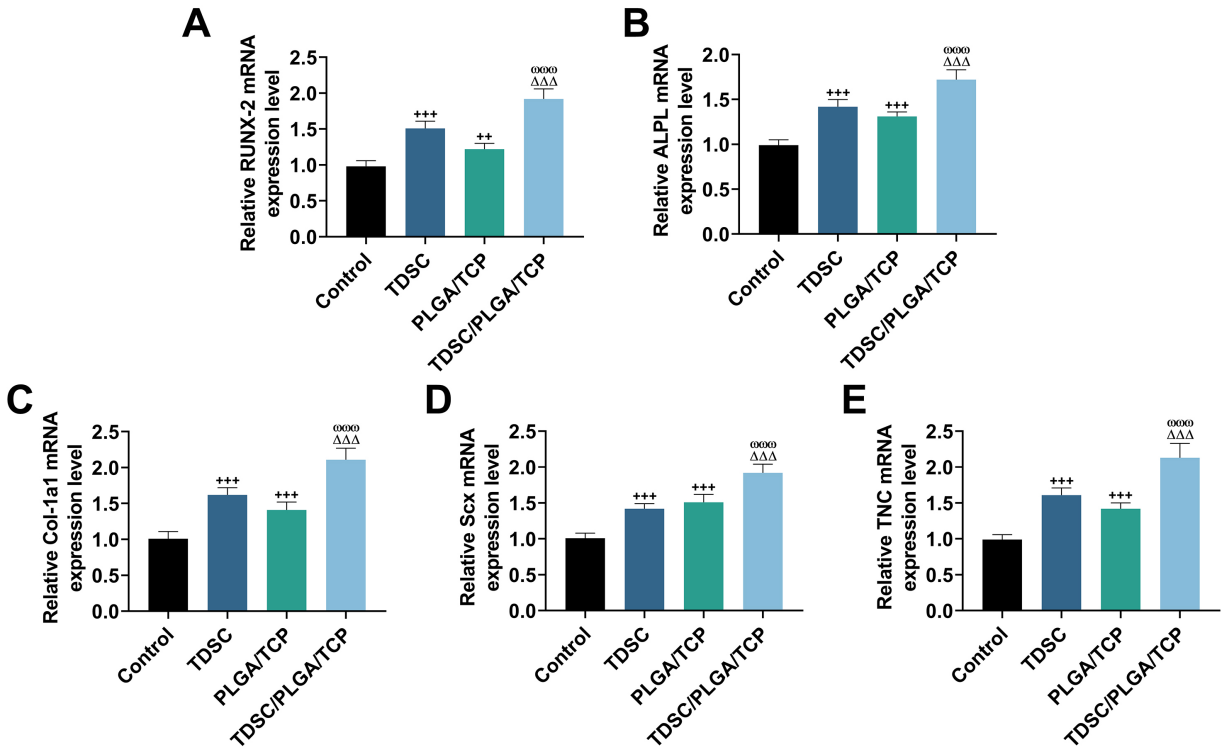

Fig. 5. TDSC/PLGA/TCP composite scaffold promotes the expressions of *RUNX-2*, *ALPL*, *COL-1a1*, *Scx,* and *TNC*. (A–E) mRNA expression levels of *RUNX-2*, *ALPL*, *COL-1a1*, *Scx,* and *TNC* in the RCT model were assessed by qRT-PCR, with *GAPDH* as the internal reference. $^{++}p < 0.01$, $^{+++}p < 0.001$ vs. Control group. $^{\Delta\Delta\Delta}p < 0.001$ vs. TDSC group. $^{\omega\omega\omega}p < 0.001$ vs. PLGA/TCP group. Each experiment was conducted eight times (n = 8).

pathway. β-catenin is a crucial effector of the Wnt signaling pathway, involving in the processes of cell proliferation and differentiation [46]. Previous research indicates that simvastatin factor-loaded silk fibroin facilitates RCT healing by activating the β-catenin signaling pathway [25]. Inhibition of Wnt/β-catenin signaling delays the healing of rotator cuff injuries [46]. Additionally, galectin-3 promotes osteogenic differentiation of precursor cells by increasing β-catenin expression in patients with skeletal hyperostosis [43]. Our findings are consistent with these previous studies, suggesting that activation of the β-catenin signaling pathway by TDSC/PLGA/TCP composite scaffold may significantly impact the osteogenic differentiation of TDSCs and RCT healing.

Furthermore, combined with our research, the PLGA/TCP scaffold loaded with TDSCs further promoted the reconstruction of the tendon-bone multilayer fibrous cartilage structure and the expressions of osteogenesis-related genes (*RUNX-2*, *ALPL*, *COL-1a1*) and tendon formation-related-genes (*Scx* and *TNC*). Previous research has shown that bone mesenchymal stem cells promote tendon-bone healing by increasing the expression of runt-related transcription factor 1 (*RUNX-1*) [47], indicating the potential significance of these genes in rotator cuff injury. Moreover, the TDSC/PLGA/TCP composite scaffold promoted β-catenin expression, the invasive number of TDSCs, and improved biomechanical properties. These findings suggest that the TDSC/PLGA/TCP composite scaffold may enhance RCT repair and tendon-done healing by modulating the β-catenin signaling pathway. However, this study lacked an in-depth analysis of the precise role of this signaling pathway in tendon-bone healing, regulation of related gene expression, and interaction with other signaling pathways. Therefore, further experiments are needed to investigate these aspects in the future.

Emerging evidence suggests that optimal treatment strategies for healing RCT and regenerating tendon-bone interface involve biomaterials and application of growth factors, stem cells, and specific treatment protocols [14]. However, the translation of these therapies into clinical practice remains slow. Furthermore, the single use of stem cells or biological scaffolds has limitations. Stem cells are ineffective in repairing bone defects, while biological scaffolds struggle to sustain cell regeneration in rotator cuff injuries [15,48]. In our study, the combined application of TDSCs and PLGA/TCP scaffold represents a novel approach to RCT repair. Therefore, compared to the traditional single use of stem cells or biological scaffolds, the TDSC/PLGA/TCP composite scaffold could address these shortcomings.

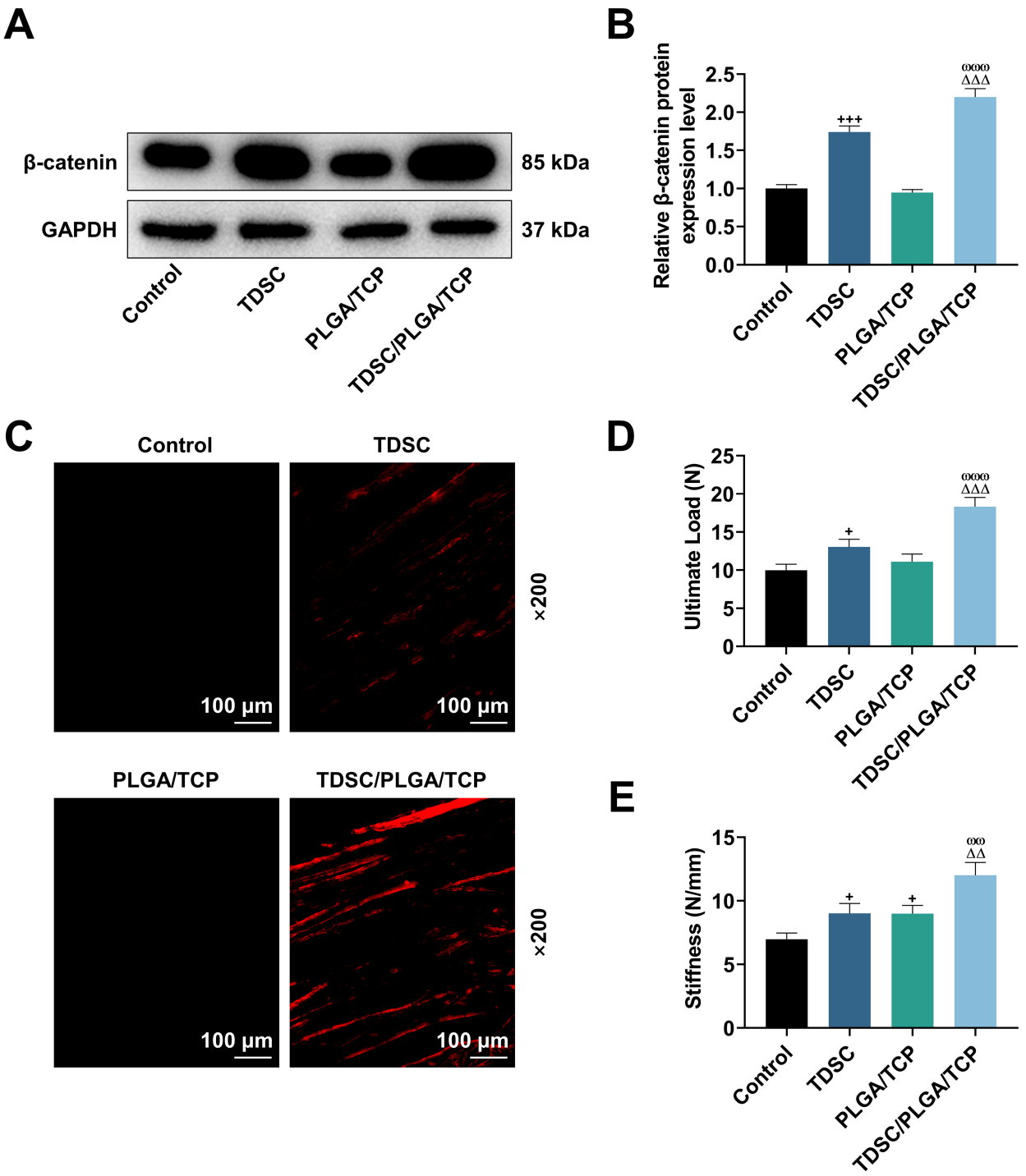

Fig. 6. TDSC/PLGA/TCP composite scaffold promotes β-catenin expression, invasive number of TDSC, ultimate load, and stiffness of healing tendon. (A,B) Protein blots of β-catenin in the RCT model were evaluated using western blot analysis, with *GAPDH* as the internal reference. (C) Assessment of the invasive number of TDSC in the RCT model was conducted through dil staining assay. Scale bar: 100 μm, magnification: ×200. (D,E) Evaluation of the ultimate load and stiffness of healing tendon in the RCT model was conducted using Tendon stretch assay. $^{+}p < 0.05$, $^{+++}p < 0.001$ vs. Control group. $^{\Delta\Delta}p < 0.01$, $^{\Delta\Delta\Delta}p < 0.001$ vs. TDSC group. $^{\omega\omega}p < 0.01$, $^{\omega\omega\omega}p < 0.001$ vs. PLGA/TCP group. Each experiment was conducted eight times (n = 8).

However, this study did not investigate the mechanical properties of the scaffold, the integration with host tissues, and the degradation rate of the scaffold. It also did not assess whether degradation products would cause inflammatory or other adverse reactions. Moreover, there was a lack of evaluation of the long-term effects and safety of stents.

Journal of
BIOLOGICAL REGULATORS
and Homeostatic Agents

In the future, it will be necessary to further explore the clinical feasibility of the TDSC/PLGA/TCP composite scaffold through clinical trials, including the assessment of clinically relevant indicators such as range of motion, strength, and pain.

Conclusions

In conclusion, our research revealed that the TDSC/PLGA/TCP composite scaffold promoted the tendon-bone healing of RCT in rabbits. Furthermore, the combination of TDSCs and PLGA/TCP scaffold appears to address the shortcomings of traditional RCT repair methods.

Availability of Data and Materials

The analyzed data sets generated during the study are available from the corresponding author on reasonable request.

Author Contributions

Substantial contributions to conception and design: WD. Data acquisition, data analysis and interpretation: LW, MB, SD, JL. Drafting the article or critically revising it for important intellectual content: All authors. Final approval of the version to be published: All authors. Agreement to be accountable for all aspects of the work in ensuring that questions related to the accuracy or integrity of the work are appropriately investigated and resolved: All authors.

Ethics Approval and Consent to Participate

All experimental operations on New Zealand white rabbits were performed in accordance with the China Council on Animal Care and Use guidelines and were approved by the Ethics Committee of Ningbo University for Experimental Animals Welfare (No. 2019-151).

Acknowledgment

Not applicable.

Funding

This work was supported by the Municipal Natural Science Foundation of Ningbo City [202003N4278]; the Ningbo Medical Key Discipline [2022-B01] and the Ningbo Top Medical and Health Research Program [2022020102].

Conflict of Interest

The authors declare no conflict of interest.

References

[1] Narvani AA, Imam MA, Godenèche A, Calvo E, Corbett S, Wallace AL, *et al*. Degenerative rotator cuff tear, repair or not repair? A review of current evidence. Annals of the Royal College of Surgeons of England. 2020; 102: 248–255.

[2] Oh JH, Park MS, Rhee SM. Treatment Strategy for Irreparable Rotator Cuff Tears. Clinics in Orthopedic Surgery. 2018; 10: 119–134.

[3] Keener JD, Patterson BM, Orvets N, Chamberlain AM. Degenerative Rotator Cuff Tears: Refining Surgical Indications Based on Natural History Data. The Journal of the American Academy of Orthopaedic Surgeons. 2019; 27: 156–165.

[4] Huang W, Dong S, Cha Y, Yuan X. SNHG11 promotes cell proliferation in colorectal cancer by forming a positive regulatory loop with c-Myc. Biochemical and Biophysical Research Communications. 2020; 527: 985–992.

[5] VanBaak K, Aerni G. Shoulder Conditions: Rotator Cuff Injuries and Bursitis. FP Essentials. 2020; 491: 11–16.

[6] Alrabaa RG, Lobao MH, Levine WN. Rotator Cuff Injuries in Tennis Players. Current Reviews in Musculoskeletal Medicine. 2020; 13: 734–747.

[7] Shao Z, Luo H, Cui G. An Efficient "M"-shaped Suturing Technique for L-shaped Rotator Cuff Tear. Arthroscopy Techniques. 2021; 10: e1655–e1659.

[8] Long Z, Nakagawa K, Wang Z, Amadio PC, Zhao C, Gingery A. Age-related cellular and microstructural changes in the rotator cuff enthesis. Journal of Orthopaedic Research: Official Publication of the Orthopaedic Research Society. 2022; 40: 1883–1895.

[9] Huang Y, Pan M, Shu H, He B, Zhang F, Sun L. Vascular endothelial growth factor enhances tendon-bone healing by activating Yes-associated protein for angiogenesis induction and rotator cuff reconstruction in rats. Journal of Cellular Biochemistry. 2020; 121: 2343–2353.

[10] Ardeljan A, Palmer J, Drawbert H, Ardeljan A, Vakharia RM, Roche MW. Partial thickness rotator cuff tears: Patient demographics and surgical trends within a large insurance database. Journal of Orthopaedics. 2019; 17: 158–161.

[11] Böhm E, Gleich J, Siebenbürger G, Böcker W, Ockert B. Rotator cuff tear: Indications and pathology-specific reconstructive procedures. Der Unfallchirurg. 2021; 124: 108–116.

[12] Imai S. Graft-Augmented Repair of Irreparable Massive Rotator Cuff Tears with Latissimus Dorsi Transfer to Treat Pseudoparesis. JB & JS Open Access. 2021; 6: e21.00044.

[13] Chen W, Sun Y, Gu X, Cai J, Liu X, Zhang X, *et al*. Conditioned medium of human bone marrow-derived stem cells promotes tendon-bone healing of the rotator cuff in a rat model. Biomaterials. 2021; 271: 120714.

[14] Zheng Y, Jia C, Jiang X, Chen J, Chen XL, Ying X, *et al*. Electroacupuncture effects on the P2X4R pathway in microglia regulating the excitability of neurons in the substantia gelatinosa region of rats with spinal nerve ligation. Molecular Medicine Reports. 2021; 23: 175.

[15] Dyrna F, Zakko P, Pauzenberger L, McCarthy MB, Mazzocca AD, Dyment NA. Human Subacromial Bursal Cells Display Superior Engraftment Versus Bone Marrow Stromal Cells in Murine Tendon Repair. The American Journal of Sports Medicine. 2018; 46: 3511–3520.

[16] Chen P, Cui L, Fu SC, Shen L, Zhang W, You T, *et al*. The 3D-Printed PLGA Scaffolds Loaded with Bone Marrow-Derived Mesenchymal Stem Cells Augment the Healing of Rotator Cuff Repair in the Rabbits. Cell Transplantation. 2020; 29: 963689720973647.

[17] Su Y, Zhang B, Sun R, Liu W, Zhu Q, Zhang X, *et al*. PLGA-based biodegradable microspheres in drug delivery: recent ad-

vances in research and application. Drug Delivery. 2021; 28: 1397–1418.

[18] Lai Y, Li Y, Cao H, Long J, Wang X, Li L, *et al*. Osteogenic magnesium incorporated into PLGA/TCP porous scaffold by 3D printing for repairing challenging bone defect. Biomaterials. 2019; 197: 207–219.

[19] Arpornmaeklong P, Pressler MJ. Effects of ß-TCP scaffolds on neurogenic and osteogenic differentiation of human embryonic stem cells. Annals of Anatomy. 2018; 215: 52–62.

[20] Gonçalves Dos Santos G, Borges Miguel IRJ, de Almeida Barbosa Junior A, Teles Barbosa W, Vieira de Almeida K, García-Carrodeguas R, *et al*. Bone regeneration using Wollastonite/β-TCP scaffolds implants in critical bone defect in rat calvaria. Biomedical Physics & Engineering Express. 2021; 7.

[21] Barreto RB, Azevedo AR, Gois MCD, Freire MRDM, Silva DS, Cardoso JC. Platelet-Rich Plasma and Corticosteroid in the Treatment of Rotator Cuff Impingement Syndrome: Randomized Clinical Trial. Revista Brasileira De Ortopedia. 2019; 54: 636–643.

[22] An B, Ji X, Gong Y. Role of CITED2 in stem cells and cancer. Oncology Letters. 2020; 20: 107.

[23] Li C, Hu X, Meng Q, Zhang X, Zhu J, Dai L, *et al*. The potential of using semitendinosus tendon as autograft in rabbit meniscus reconstruction. Scientific Reports. 2017; 7: 7033.

[24] Fu G, Lu L, Pan Z, Fan A, Yin F. Adipose-derived stem cell exosomes facilitate rotator cuff repair by mediating tendon-derived stem cells. Regenerative Medicine. 2021; 16: 359–372.

[25] Hao L, Chen J, Shang X, Chen S. Surface modification of the simvastatin factor-loaded silk fibroin promotes the healing of rotator cuff injury through β-catenin signaling. Journal of Biomaterials Applications. 2021; 36: 210–218.

[26] Hohmann E. Editorial Commentary: Tendon-Derived Stem Cells Are in the Rotator Cuff Remnant and Decline With Age and Tear Chronicity-But the Clinical Relevance Is Not Known. Arthroscopy: the Journal of Arthroscopic & Related Surgery: Official Publication of the Arthroscopy Association of North America and the International Arthroscopy Association. 2022; 38: 1049–1050.

[27] Turturici M, Roatta S. Effects of gadolinium chloride on basal flow and compression-induced rapid hyperemia in the rabbit masseter muscle. Journal of Physiology and Pharmacology: an Official Journal of the Polish Physiological Society. 2014; 65: 409–415.

[28] Omi R, Gingery A, Steinmann SP, Amadio PC, An KN, Zhao C. Rotator cuff repair augmentation in a rat model that combines a multilayer xenograft tendon scaffold with bone marrow stromal cells. Journal of Shoulder and Elbow Surgery. 2016; 25: 469–477.

[29] Huang Y, He B, Wang L, Yuan B, Shu H, Zhang F, *et al*. Bone marrow mesenchymal stem cell-derived exosomes promote rotator cuff tendon-bone healing by promoting angiogenesis and regulating M1 macrophages in rats. Stem Cell Research & Therapy. 2020; 11: 496.

[30] Xie XH, Wang XL, Zhang G, He YX, Leng Y, Tang TT, *et al*. Biofabrication of a PLGA-TCP-based porous bioactive bone substitute with sustained release of icaritin. Journal of Tissue Engineering and Regenerative Medicine. 2015; 9: 961–972.

[31] Kleim BD, Siebenlist S, Scheiderer B, Imhoff AB. Irreparable rotator cuff tear-reverse shoulder arthroplasty and alternative procedures. Der Unfallchirurg. 2021; 124: 117–124.

[32] Longo UG, Carnevale A, Piergentili I, Berton A, Candela V, Schena E, *et al*. Retear rates after rotator cuff surgery: a systematic review and meta-analysis. BMC Musculoskeletal Disorders. 2021; 22: 749.

[33] Porschke F, Schlee SM, Schnetzke M, Studier-Fischer S, Gruetzner PA, Guehring T. Functional outcome and tendon integrity of rotator cuff reconstruction after primary traumatic glenohumeral dislocation. Archives of Orthopaedic and Trauma Surgery. 2020; 140: 1073–1079.

[34] Tarafder S, Brito JA, Minhas S, Effiong L, Thomopoulos S, Lee CH. In situ tissue engineering of the tendon-to-bone interface by endogenous stem/progenitor cells. Biofabrication. 2019; 12: 015008.

[35] K N, Ca V, Joseph J, U A, John A, Abraham A. Mesenchymal Stem Cells Seeded Decellularized Tendon Scaffold for Tissue Engineering. Current Stem Cell Research & Therapy. 2021; 16: 155–164.

[36] Liu F, Meng Q, Yin H, Yan Z. Stem Cells in Rotator Cuff Injuries and Reconstructions: A Systematic Review and Meta-Analysis. Current Stem Cell Research & Therapy. 2019; 14: 683–697.

[37] Xu Y, Zhang WX, Wang LN, Ming YQ, Li YL, Ni GX. Stem cell therapies in tendon-bone healing. World Journal of Stem Cells. 2021; 13: 753–775.

[38] Lui PPY, Wong CM. Biology of Tendon Stem Cells and Tendon in Aging. Frontiers in Genetics. 2020; 10: 1338.

[39] Campbell TM, Lapner P, Dilworth FJ, Sheikh MA, Laneuville O, Uhthoff H, *et al*. Tendon contains more stem cells than bone at the rotator cuff repair site. Journal of Shoulder and Elbow Surgery. 2019; 28: 1779–1787.

[40] Sevivas N, Teixeira FG, Portugal R, Direito-Santos B, Espregueira-Mendes J, Oliveira FJ, *et al*. Mesenchymal Stem Cell Secretome Improves Tendon Cell Viability *In Vitro* and Tendon-Bone Healing *In Vivo* When a Tissue Engineering Strategy Is Used in a Rat Model of Chronic Massive Rotator Cuff Tear. The American Journal of Sports Medicine. 2018; 46: 449–459.

[41] Kim W, Kim GE, Attia Abdou M, Kim S, Kim D, Park S, *et al*. Tendon-Inspired Nanotopographic Scaffold for Tissue Regeneration in Rotator Cuff Injuries. ACS Omega. 2020; 5: 13913–13925.

[42] Sun F, Sun X, Wang H, Li C, Zhao Y, Tian J, *et al*. Application of 3D-Printed, PLGA-Based Scaffolds in Bone Tissue Engineering. International Journal of Molecular Sciences. 2022; 23: 5831.

[43] Xu L, Qian Z, Wang S, Wang R, Pu X, Yang B, *et al*. Galectin-3 Enhances Osteogenic Differentiation of Precursor Cells From Patients With Diffuse Idiopathic Skeletal Hyperostosis via Wnt/β-Catenin Signaling. Journal of Bone and Mineral Research: the Official Journal of the American Society for Bone and Mineral Research. 2022; 37: 724–739.

[44] Peng X, He J, Zhao J, Wu Y, Shi X, Du L, *et al*. Polygonatum Sibiricum Polysaccharide Promotes Osteoblastic Differentiation Through the ERK/GSK-3β/β-Catenin Signaling Pathway *In Vitro*. Rejuvenation Research. 2018; 21: 44–52.

[45] Rak Kwon D, Jung S, Jang J, Park GY, Suk Moon Y, Lee SC. A 3-Dimensional Bioprinted Scaffold With Human Umbilical Cord Blood-Mesenchymal Stem Cells Improves Regeneration of Chronic Full-Thickness Rotator Cuff Tear in a Rabbit Model. The American Journal of Sports Medicine. 2020; 48: 947–958.

[46] Xu QM, Fang F, Wu SH, Shi ZQ, Liu Z, Zhoa YJ, *et al*. Dendritic cell TLR4 induces Th1-type immune response against Cryptosporidium parvum infection. Tropical Biomedicine. 2021; 38: 172–179.

[47] Kang K, Geng Q, Cui L, Wu L, Zhang L, Li T, *et al*. Upregulation of Runt related transcription factor 1 (RUNX1) contributes to tendon-bone healing after anterior cruciate ligament reconstruction using bone mesenchymal stem cells. Journal of Orthopaedic Surgery and Research. 2022; 17: 266.

[48] Yuan Z, Cao F, Gao C, Yang Z, Guo Q, Wang Y. Decellularized Human Umbilical Cord Wharton Jelly Scaffold Improves Tendon Regeneration in a Rabbit Rotator Cuff Tendon Defect Model. The American Journal of Sports Medicine. 2022; 50: 371–383.